A surrogate model for uncertainty quantification and global sensitivity analysis of nonlinear large-scale dome structures

Huidong Zhang[1,2*], Yafei Song[1], Xinqun Zhu[3], Yaqiang Zhang[1], Hui Wang[1], Yingjun Gao[1]

[1]School of Civil Engineering, Tianjin Chengjian University, Tianjin 300384, China

[2]Tianjin Key Laboratory of Civil Building Protection and Reinforcement, Tianjin 300384, China

[3]School of Civil and Environmental Engineering, University of Technology Sydney, NSW 2007, Australia

Abstract: Full-scale dome structures have numerous sources of aleatoric uncertainty that are irreducible due to their intrinsic nature. When using the finite element method (FEM) to quantify the effects of these sources on structural dynamic performance, a large-scale numerical simulation of dome structure is required. To reduce the heavy computational burden, a surrogate model for a dome structure is constructed to solve this problem in this paper. The dynamic global sensitivity of elastic and elastoplastic structures is analyzed in the uncertainty quantification framework using fully quantitative variance- and distribution-based methods through the surrogate model, which takes into account the main sources of uncertainty related to the dome structure that have an important influence on structural performance. The effects of variables on structural performance indicators are quantified using sthe ensitivity index values of different performance states. Finally, the effects of sample sizes and correlation functions on the accuracy of the surrogate model, and the effects of surrogate accuracy and failure probability on sensitivity index values are discussed. The results show that the surrogate modelling has a high computational efficiency and acceptable accuracy in the uncertainty quantification of large-scale structures under earthquakes when compared to conventional FEM.

Keywords: large-scale dome structures; surrogate model; global sensitivity analysis; uncertainty quantification; structural performance.

1. Introduction

There are numerous uncertainties in engineering structures, which mainly include [1, 2]: (1) the shape of the real structure is not completely consistent with the design due to human errors in the construction process; (2) the members may have an initial small deformation due to manufacturing errors; (3) the real material properties may differ slightly with that used in the design; (4) the idealized loading in the numerical modelling is used to roughly represent the real loading; and (5) the damping characteristics that affect structural dynamic behaviour are difficult to quantify with certainty in dynamic cases. These sources of uncertainty are either aleatoric or epistemic. The effects of some uncertainties on structural performance have been considered indirectly in current specifications and a deterministic analysis strategy is adopted in the uncertainty quantification. As these uncertainties are random variables in nature, they cannot be explicitly characterized in the results. Quantifying their possible effects on structural performance is necessary as they are not yet fully understood.

This paper focuses on aleatoric uncertainty. The probability theory is an excellent tool to describe characteristics of aleatoric sources of uncertainty by means of probability density functions (PDFs). For stochastic structural modelling , two techniques are now used: completely random modelling [1, 2] and globally random modelling [3]. The former needs more complex modelling procedures, whereas the latter is a more efficient way to evaluate the performance of a structure with uncertainties since each variable is taken into account for the entire structure. To quantify the effects of the sources of uncertainty on the structural performance, the global sensitivity analysis (GSA) plays a critical role, and the globally random modelling method for sensitivity analysis is suitable.

*Corresponding author: Huidong Zhang, School of Civil Engineering, Tianjin Chengjian University, Tianjin 300384, China

E-mail: zhhuidong@126.com

The GSA has been used for the model simplification, importance ranking, risk reduction, and data process management recently [4]. The applications of the GSA for engineering structures can be summarized as [5-8]: (1) understanding the input-output relationship to explore causalities; (2) determining the contribution of variables to the results for reducing the potential uncertainty; (3) identifying important variables for the dimensionality reduction; and (4) support the decision-making to guide future designs.

There are several methods to conduct the GSA, including [9] the derivative-based, variance-based, distribution-based, and regression-based approaches. In the last decade, the variance-based approach for GSA has received more attention in the field of civil engineering. Using the variance-based method, Nariman et al. [10] assessed the effects of variables on the tensile damage and stability of a tunnel structure subjected to earthquakes. Zoutat et al. [11] used the variance-based method to determine the contribution of variables to the lateral displacement of a frame structure. Menz and Dubreuil [12] developed a method for quantifying the sensitivity of failure probability to the variables in the framework for variance-based analysis. To quantitatively analyse the effects of variables on the results, Zhang et al. [13] performed an analytical derivation of global sensitivity for models with variables based on the variances of variables, indicating that the analytical solution could be used in practice. Javidan and Kim [14] validated the efficiency of the variance-based GSA for fuzzy structural systems. Other developments for GSA can be found in the literature [15-17]. However, it has been reported [18] that in GSA, distribution-based techniques may be more robust than variance-based techniques when the sensitivity is described by the differences of the output distributions rather than just variances only. By combining variance-based and distribution-based approaches, Baroni and Francke [19] developed an effective strategy for GSA. From the above studies, the computational burden for the GSA of complex structures is enormous. It limited their practical applications, particularly for nonlinear structures.

The meta-learning method, one of the fastest-growing research areas in machine learning, has been used to reduce the computing burden in GSA. Wei et al. [20] developed a GSA method based on the Karhunen-Loeve (KL) expansion, and the method was used to identify the contribution of the variables to the structural reliability. Ni et al. [21] presented a sensitivity analysis and uncertainty quantification for the natural frequencies and dynamic responses of a bridge structure based on the polynomial chaos expansion (PCE). Another popular method for quantifying uncertainty in design optimization [22] and model updating [23] is the Kriging model. To choose parameters in stochastic model updating, Yuan et al. [24] integrated the Kriging surrogate model with GSA. Wan and Ni [25] investigated the effect of variables on the dynamic demands of a time-varying structure system using an analytical Gaussian regression model. Amini et al. [26] investigated the superiority of the polynomial chaos Kriging (PCK) metamodel in quantifying the uncertainty of dam structures over other conventional methods. It is still a big challenge to use the meta-learning method for cases with complex structures and excitations.

In previous studies, the statistical sensitivity analysis, including GSA, is performed directly in large-scale dome systems using sampling methods. Taking into account the uncertain sources in the large-scale single-layer dome, Zhang et al. [1, 2] used the Monte Carlo sampling (MCS) method to construct a sensitivity analysis of the structural seismic performance based on the variance of structural demands. Xian et al. [27] performed a stochastic sensitivity analysis for structures with viscous dampers during earthquakes using Monte Carlo simulation. Because the collapse behaviour of double-layer dome structures varies depending on random factors, Vaezi Vazna and Zarrin [28] carried out the sensitivity analysis and used the First-Order-Second-Moment (FOSM) method to assess the importance of uncertain parameters. Using an MCS method and a Gaussian process metamodel, Wan and Ren [29] proposed a

GSA method for solving parameter selection problems for an arch bridge. All the above, the finite element model was used and the computational burden is a challenge for practical applications. Recently, Sun and Dias [30] used a sparse PCE to build a surrogate model for performing the GSA of seismic deformation of a soil tunnel.

In previous studies, the finite element method was mostly used in GSA of large-scale structures, the computational efficiency is low, and the GSA is for elastic structures. This study extends to elastoplastic structures subjected to complex stochastic excitations using an efficient regression-Kriging surrogate model method. The variance- and distribution-based approaches are used to quantify the importance of several variables. The effects of some key factors on the accuracy of the surrogate model and sensitivity index values are also discussed in this paper.

2. Surrogate modelling and GSA method for structures

2.1 Surrogate modelling

A surrogate model of a structure can be represented mathematically as

$$\widehat{\boldsymbol{y}} = \varphi(\boldsymbol{x}; [\boldsymbol{x_t}, \boldsymbol{y_t}]) \tag{1}$$

where $\boldsymbol{x} \in \Re^n$ represents the n input variables, $\boldsymbol{x_t} \in \Re^{m\times n}$ is the training input vector, $\boldsymbol{y_t} \in \Re^m$ is the training output vector, $\widehat{\boldsymbol{y}}$ is the prediction for the true value vector $\boldsymbol{y}$, and $\varphi(\cdot)$ is the surrogate model constructed using $\boldsymbol{x_t}$ and $\boldsymbol{y_t}$. To construct the surrogate model of a structure, training samples $[\boldsymbol{x_t}, \boldsymbol{y_t}]$ must be obtained using physics-based methods such as the finite element method. After constructing the surrogate model, $\boldsymbol{y}$ can be quickly estimated for a continuous spatial field using this surrogate model, allowing the uncertainty quantification and GSA to be carried out efficiently.

The regression-Kriging (RK) method [31], a hybrid interpolation technique, is introduced in this paper to construct the mapping function of a structure with variables obeying normal distributions because it can well describe the global and local characteristics of the sample data and is easily implemented to reduce the computational burden.

According to the RK model, the output y can be written as,

$$y=\sum_{i=1}^{p} \beta_i f_i(x) + \epsilon(x) \tag{2}$$

where β_i and $\boldsymbol{f_i}(x)$ are the ith regression coefficient and regression function, respectively, $\sum_{i=1}^{p} \beta_i f_i(x)$ represents global approximations for y and can be estimated using a quadratic model to improve regression accuracy, and $\epsilon(x)$ reflects the local deviations of y, which is defined as a stochastic process with a mean of zero and a variance of σ^2. The covariance matrix of $\epsilon(x)$ is written as

$$cov\left[\epsilon(x_i), \epsilon\left(x_j\right)\right] = \sigma^2 \mathbf{R}[R\left(\theta; x_i, x_j\right)] \tag{3}$$

where $R(\cdot)$ is the correlation function, θ is a parameter, and $\mathbf{R} \in \Re^{m\times m}$ is the correlation function matrix. There are some correlation functions available, including the exponential, Gaussian, Matérn linear, and Matérn cubic functions. The Gaussian correlation function is the most commonly used,

$$R\left(\theta; x_i, x_j\right) = \prod \exp\left(-\theta_k (x_{ik} - x_{jk})^2\right),\ \forall \theta_k \in \Re^+ \tag{4}$$

where θ_k is the kth unknown to be determined. Here the Matérn 3/2 correlation function is used for the surrogate modelling of elastoplastic structures and the correlation function is expressed as [32]

$$R\left(\theta; x_i, x_j\right) = \prod(1 + \sqrt{3}\theta_k \left|x_{ik} - x_{jk}\right|)\exp\left(-\sqrt{3}\theta_k \left|x_{ik} - x_{jk}\right|\right),\ \forall \theta_k \in \Re^+ \tag{5}$$

Assuming that the known sample points are denoted as $[\boldsymbol{s}^m, \boldsymbol{Y}^m]$ and $\boldsymbol{s}$ follows the standard normal distribution. According to the RK model, the prediction $\hat{y}(\boldsymbol{u})$ for an untried sample set $\boldsymbol{u}$ can be written as [31],

$$\hat{y}(\boldsymbol{u}) = \beta^* + r(\boldsymbol{u})^T R^{-1}(\boldsymbol{Y} - \boldsymbol{f}\beta^*) \tag{6}$$

where β^* is a constant, $r(\boldsymbol{u})$ is the vector of correlation values between $\boldsymbol{u}$ and $\boldsymbol{s}$, $\mathbf{R}$ is the

correlation function matrix of the known sample vector $\boldsymbol{s}$, and $\boldsymbol{f}$ is the regression function vector. β^* can be calculated using the following formula,

$$\beta^* = (\boldsymbol{f}^T R^{-1} \boldsymbol{f})^{-1} \boldsymbol{f}^T R^{-1} \boldsymbol{Y} \tag{7}$$

and the estimated variance is written as,

$$\sigma^{*2} = \frac{1}{m} (\boldsymbol{Y} - \boldsymbol{f}\beta^*)^T R^{-1} (\boldsymbol{Y} - \boldsymbol{f}\beta^*) \tag{8}$$

The optimum estimate for θ_k can be obtained by maximizing the likelihood estimate,

$$ln(L) \approx \frac{m ln(\sigma^{*2}) + ln|R|}{2} \tag{9}$$

More information is available in the literature [31].

A surrogate model is constructed using the method described above. Given the high nonlinearity in structures, the prediction performance of surrogate models should be evaluated using an error metric (Q^2),

$$Q^2 = 1 - \frac{\sum_{i=1}^{k} (y_i - \hat{y}_i)^2}{\sum_{i=1}^{k} (y_i - \bar{y})^2} \tag{10}$$

where k is the sample size, and $\hat{y}_i$ and $\bar{y}$ are the prediction and mean of y_i, respectively. The closer the value of Q^2 is to 1, the better the regression effect and the prediction accuracy of the surrogate model. When the value of Q^2 exceeds 0.8, the surrogate model is usually appropriate for GSA. The mean square error MSE is another metric for assessing the accuracy of the surrogate model,

$$MSE = \frac{\sum_{i=1}^{k} (y_i - \hat{y}_i)^2}{k} \tag{11}$$

2.2 GSA methods

The output $\hat{y}(\boldsymbol{x})$ can be obtained after the sample set of $\boldsymbol{x}$ has been determined using the Latin hypercube samping (LHS) method. $\hat{y}(\boldsymbol{x})$ can be written as,

$$\hat{y}(\boldsymbol{x}) = \hat{y}_0 + \sum_{i=1}^{n} \hat{y}_i(x_i) + \sum_{1 \le i < j \le n} \hat{y}_{ij}(x_i, x_j) + \cdots + \hat{y}_{12\ldots n}(x_1, x_2, \ldots, x_n) \tag{12}$$

where $\hat{y}_0$ is the mean value of $\hat{y}(\boldsymbol{x})$, and $\hat{y}_i(x_i)$, $\hat{y}_{ij}(x_i, x_j)$, and $\hat{y}_{12\ldots n}(x_1, x_2, \ldots, x_n)$ represent the first-order, second-order, and high-order components, respectively. Due to the orthogonality, the unconditional variance of $\hat{y}(\boldsymbol{x})$ can be decomposed as,

$$V(\hat{y}) = \sum_i V_i + \sum_{1 \le i < j \le n} V_{ij} + \cdots + V_{12\ldots n} \tag{13}$$

where V_i is the contribution to the variance of $\hat{y}(\boldsymbol{x})$ of single variable x_i, V_{ij} is the contribution of the interactions between x_i and x_j, and $V_{12\ldots n}$ is the high-order contribution. Here, V_i and V_{ij} can be written as [7, 33],

$$\begin{cases} V_i = V[\mathbb{E}(\hat{\boldsymbol{y}}|x_i)] \\ V_{ij} = V\left[\mathbb{E}\left(\hat{\boldsymbol{y}}|x_i, x_j\right)\right] - V[\mathbb{E}(\hat{\boldsymbol{y}}|x_i)] - V[\mathbb{E}(\hat{\boldsymbol{y}}|x_j)] \end{cases} \tag{14}$$

Thus, the decomposition of sensitivity indices can be expressed as,

$$1 = \sum_i S_i + \sum_{1 \le i < j \le n} S_{ij} + \cdots + S_{12\ldots n} \tag{15}$$

where $S_i = V_i / V(\hat{y})$ is the first-order sensitivity index, and $S_{ij} = V_{ij} / V(\hat{y})$ is the second-order sensitivity index. The total sensitivity index can be written as [34],

$$S_{Ti} = 1 - \frac{V_{\sim i}[\mathbb{E}(\hat{\boldsymbol{y}}|x_{\sim i})]}{V(\hat{\boldsymbol{y}})} \tag{16}$$

where $\mathbb{E}(\hat{\boldsymbol{y}}|x_{\sim i})$ is the mean value of $\hat{\boldsymbol{y}}$ when keeping all parameters but x_i fixed, and $V_{\sim i}[\mathbb{E}(\hat{\boldsymbol{y}}|x_{\sim i})]$ is its variance.

The total-order index of a variable reflects the effects of this variable and its interactions with all other variables on the output [34], while the first-order index of the variable evaluates the main effect of the

variable on the output, and the second-order index evaluates the interactive effect between two variables, and so forth. The difference of $S_{Ti} - S_i$ represents the degree of the interactions between the variable x_i and the other variables. The higher-order coupling effects are not discussed in this paper because the index values are small.

Another GSA method that has attracted the attention of researchers recently is based on probability distributions, including probability distributions based on the variables and probability distributions based on the outputs. In engineering structures, the structural failure function $G(\boldsymbol{X})$ is commonly expressed as,

$$G(\boldsymbol{x}) = D_0 - |A_i|_{max} \tag{17}$$

where D_0 and $|A_i|_{max}$ are the critical value and the maximum demand of the i^{th} sampling structure, respectively. Once D_0 is defined, it is obvious that the values of $G(\boldsymbol{x})$ may be divided into two subsets: $G(\boldsymbol{x}) \leq 0$ and $G(\boldsymbol{x}) > 0$. The effect of a variable on the output can be determined by comparing the difference between the unconditional PDF $f_{x_i}(x_i)$ and the conditional PDF $f_{x_i}(x_i|Failure)$ in the sample set of variables. As a result, the index S_i of the variable is defined as [35],

$$S_i = \frac{1}{2}\int \left| f_{x_i}(x_i) - f_{x_i}(x_i|Failure) \right| dx_i \tag{18}$$

S_i represents the first-order global sensitivity index, whose value ranges from 0 to 1. The high value of S_i shows that the variable x_i has a great effect on structural failure. Since it may directly estimate the importance ranking of variables [35, 36], only this index is discussed in the distribution-based method. It should be noted that, due to different theoretical viewpoints, the variance-based method and the distribution-based method are numerically incomparable; however, the importance ranking of variables provided by the two is comparable.

The conditional PDF is non-parametrized and cannot be easily estimated using the existing parametrized density functions. The PDFs in this paper are estimated using the kernel smoothing method. The kernel-smoothed PDF is expressed as [37],

$$\hat{p}(x) = \frac{1}{Nh}\sum_{i=1}^{N} K_e\left(\frac{x - x_i}{h}\right) \tag{19}$$

where $K_e(\cdot)$, N, x_i, and h are the univariate kernels, sample size, i^{th} sample value, and bandwidth, respectively, and $\int K_e(x)dx = 1$. The kernel function $K_e(x)$ is a symmetric PDF. The optimal bandwidth is determined using the plug-in bandwidth selection method in this paper, and the fitting effect is controlled by the asymptotic mean integrated square error (AMISE) criterion.

3. Validation

The analysis strategy described above is developed in a Python development environment. To validate the methods, the Ishigami function from the literature [38] is used to investigate nonlinear problems,

$$f(x) = sin(x_1) + asin^2(x_2) + bx_3^4 sin\,(x_1) \tag{20}$$

where $x_i \in [-\pi, \pi]$ for $i = 1, 2, 3$. x_1, x_2, and x_3 are independent and have a uniform marginal distribution. Furthermore, a and b are set to 7 and 0.1, respectively. The function is highly nonlinear and nonmonotonic. It also has a peculiar dependence on x_3. The theoretical values of the first-order Sobol indices are as follows [39],

$$S_1 = \frac{V_1}{V}, S_2 = \frac{V_2}{V}, S_3 = 0 \tag{21}$$

where $V = \frac{1}{2} + \frac{a^2}{8} + \frac{b^2\pi^8}{18} + \frac{b\pi^4}{5}$, $V_1 = \frac{1}{2}\left(1 + b\frac{\pi^4}{5}\right)^2$, $V_2 = \frac{a^2}{8}$, and $V_{1,3} = b^2\pi^8\frac{8}{225}$. The values of the total-order indices are expressed as [39],

$$S_{T1} = \frac{V_1 + V_{1,3}}{V}, S_{T2} = S_2, S_{T3} = \frac{V_{1,3}}{V} \tag{22}$$

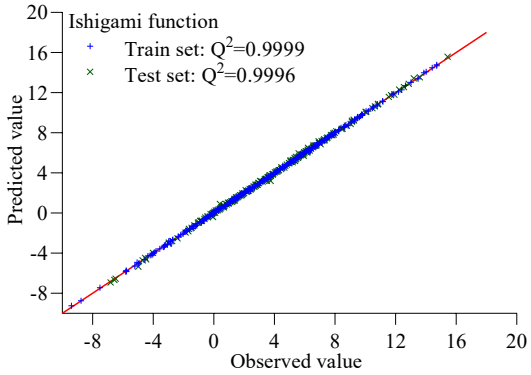

Fig. 1 Q^2 values of the training and test sets

The sample size is set to 1000 in the current analysis, with a training set of 700 samples used to assess statistical uncertainty and construct the surrogate model of the Ishigami function, and a test set of 300 samples used to validate the surrogate model. Fig. 1 depicts the Q^2 values of the training and test sets. Because the points are almost on the diagonal of the first quadrant, these values are very close to 1, indicating that the constructed surrogate model is excellent and has good predictability.

Table 1 Sensitivity index values

Index S_i	S_1	S_2	S_3
Theoretical values	0.3139	0.4425	0.0
Variance-based	0.3139	0.4426	0.0
Distribution-based	0.5124 (1)	0.4201 (2)	0.2286 (3)
Index S_{Ti}	S_{T1}	S_{T2}	S_{T3}
Theoretical values	0.5575 (1)	0.4425 (2)	0.2437 (3)
Variance-based	0.5574 (1)	0.4426 (2)	0.2435 (3)

The GSA for the Ishigami function is performed using variance-based and distribution-based methods based on this surrogate model. Table 1 lists the theoretical values, the values obtained using the two methods, and the importance ranking of the variables. The first-order and total-order Sobol index values in the variance-based method are found to be in good agreement with the theoretical values, and both methods provide the same results in terms of the importance ranking of the variables.

The values in the samples are preprocessed using min-max normalization to improve the accuracy of the estimated index values in the distribution-based method. Fig. 2 depicts the histograms of the variables in the failure set, fitted conditional PDFs, and original PDFs. The fitted conditional PDFs using the kernel smoothing method agree well with the histograms and can describe the characteristics of the variables in the failure set.

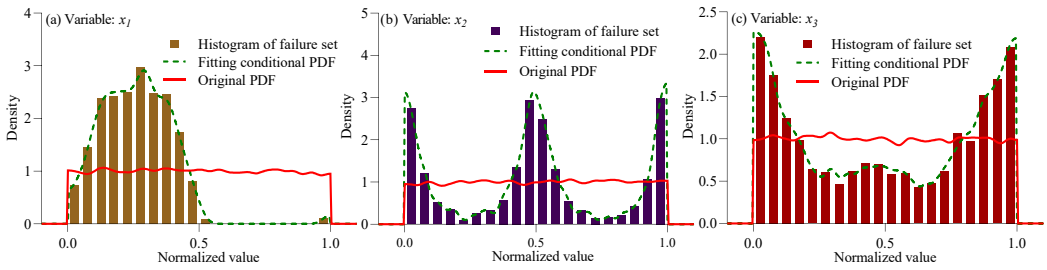

Fig. 2 Conditional PDFs and unconditional PDFs

4. A large-scale single-layer dome

4.1 Model

A large-scale single-layer dome [40] with a span length of 121.5 m, a height of 24.2 m, and a span-height ratio of 5:1 is shown in Fig. 3. 756 pipe members of the structure are regularly connected by 271

joints. The external diameter of each pipe member is 0.245 m, and the wall-thickness is 0.01 m. The yielding strength and strain-hardening ratio of the steel material are set at 345 MPa and 0.015, respectively. The elastic modulus is set to 2.06e11 Pa. According to the equivalence, the uniformly distributed roof mass is applied to each joint as a concentrated mass, and each joint has a mass of 9471 kg. The joints at the base of the structure are completely fixed.

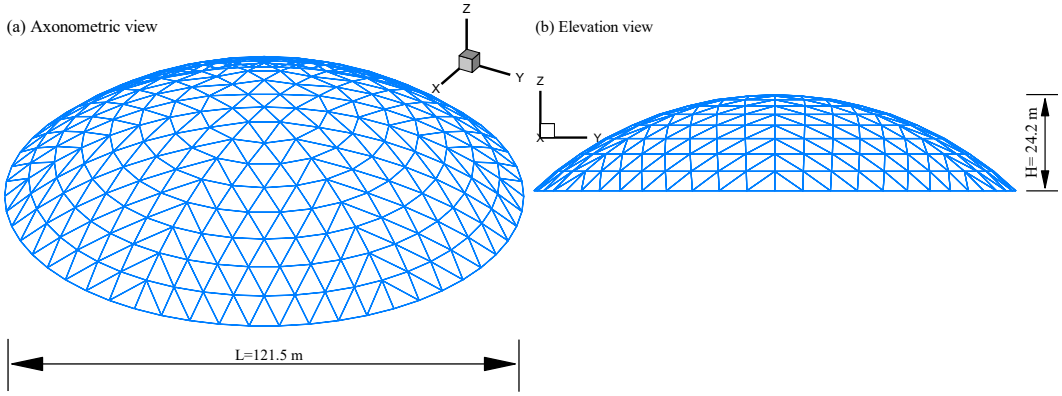

Fig. 3 Structural model: (a) Axonometric view; (b) Elevation view

The structural finite element model with variables is developed in the probabilistic framework with the OpenSees program, which is based on a command-driven format and parameterized modelling method. Each pipe member is modelled using a displacement-based beam-column element with a fibre cross-section model. In the circumferential and radial directions, the cross-section is divided into 20 fibres and 3 fibres, respectively. As a result, the finite element model has 756 elements and 271 nodes. The Giuffré-Menegotto-Pinto model with isotropic strain hardening is used to model the elastoplastic stress-strain relationship of the steel material. The large-deformation effect is considered in the modelling because of the shape and size of the structure. The structural damping ratio is 0.02. To model the damping force in the structure, the Rayleigh damping model is used, with the circular frequencies of the two modes for determining the damping coefficients α and β and set to 0.667 and 3.0 times the structural first-order circular frequency, respectively. Static analysis is performed before dynamic analysis. In comparison to previous studies, this study considers both geometric and material nonlinearity, making high-accuracy surrogate modelling difficult.

Table 2 summarizes and lists the statistical characteristics of variables in the dome based on the related literature [1, 2, 29]. The structural failure function for single-layer domes can be expressed as [1],

$$G(\boldsymbol{x}_{1,\dots,}\boldsymbol{x}_n) = L/n_D - |D_i|_{max} \tag{23}$$

where $\boldsymbol{x}_1, \dots, \boldsymbol{x}_n$ are n variables in the dome, L is the span length, $|D_i|_{max}$ is the maximum vertical deformation (MVD) in the i^{th} sampling dome during an earthquake, and n_D is a constant that is defined by the limit states.

Table 2 Variables for sensitivity analysis

Variable ($\boldsymbol{X}$)	Mean ($\boldsymbol{\mu}$)	Sd ($\boldsymbol{\sigma}$)	Bound	Distribution
Elastic modulus, E/Pa	μ=2.06e11	0.05× μ	$\{\mu-\sigma, \mu+\sigma\}$	$X_b \sim Norm(\mu, \sigma)$
Yield strength, f_y/Pa	$\mu = 345e6$	0.05× μ		
Strain-hardening ratio, b	$\mu = 0.015$	0.05× μ		
Wall-thickness of the member, t_w/m	$\mu = 0.01$	0.05× μ		
Node load, N_l/kg	$\mu = 9471.0$	0.1× μ		
Damping ratio, ξ	$\boldsymbol{\mu = 0.02}$	0.3× $\boldsymbol{\mu}$		

4.2 Ground motion records

Ground motions are critical in structural dynamic analysis. The ground motions used in numerical modelling are currently based primarily on natural earthquake records obtained from strong ground motion databases such as the PEER Strong Ground Motion Databases. Natural ground motion records, on the other hand, differ in duration, time step, spectrum characteristic, peak acceleration, etc. An artificial way of generating ground motions is used to fully reflect the spectrum characteristics of all the chosen natural ground motions. Table 3 lists 10 typical far-field and near-field natural earthquake records from the PEER strong earthquake databases. Fig. 4 shows the spectra in three directions as well as their mean spectra (target spectra).

Table 3 Natural earthquake records

Event	Station	Year	PGA		
			x/(m/s^2)	y/(m/s^2)	z/(m/s^2)
Coalinga-01	Parkfield-Cholame 12W	1983	0.0436	0.0468	0.0219
Imperial Valley-06	Compuertas	1979	0.1866	0.1471	0.0735
Kobe, Japan	Shin-Osaka	1995	0.225	0.2333	0.0635
Kocaeli, Turkey	Arcelik	1999	0.2101	0.1342	0.0828
Landers	Yermo Fire Station	1992	0.2445	0.1517	0.1359
Loma Prieta	Hollister-South & Pine	1989	0.3699	0.1787	0.1975
Morgan Hill	Capitola	1984	0.0988	0.1419	0.0449
Northridge-01	Covina-W Badillo	1994	0.1047	0.0817	0.0438
Superstition Hills-02	El Centro Imp. Co. Cent	1987	0.3573	0.2595	0.1276
Westmorland	Parachute Test Site	1981	0.2321	0.1489	0.1513

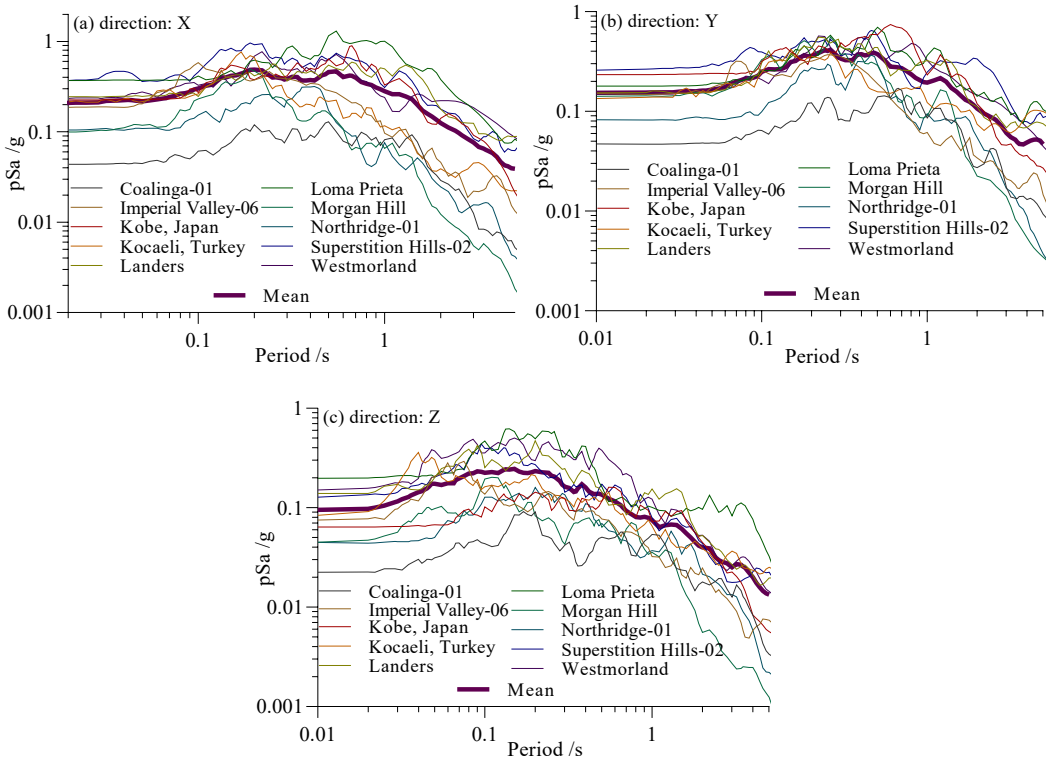

Fig. 4 Spectra of 10 earthquake records and their mean spectra

The following formula was proposed by Kaul [41] for converting the target response spectrum to the corresponding power spectral density,

$$S_x(\omega_k) = -\frac{\xi}{\pi\omega_k} \cdot \frac{[S_\alpha^T(\omega_k)]^2}{\ln(\frac{-\pi}{\omega_k T_d}\ln(1-e))} \tag{24}$$

where $S_\alpha^T(\omega_k)$ is the target response spectrum, ξ is the damping ratio, T_d is the ground motion duration, and e is the exceeding probability of the target response spectrum; typically, the value of e

is less than 15%. Furthermore, ξ and T_d are set to 2% and 20 s in this paper, respectively.

The stationary Gaussian process $\alpha(t)$ can be obtained using the trigonometric series method [42],

$$\alpha(t) = \sum_{k=1}^{N} C_k \cos(\omega_k t + \varphi_k) \tag{25}$$

where $C_k = \sqrt{4S_x(\omega_k)\Delta\omega}$, $\Delta\omega = (\omega_u - \omega_l)/N$, $\omega_k = \omega_l + (k - 1/2)\Delta\omega$, and φ_k is the random phase angle uniformly distributed in $(0, 2\pi)$, and ω_u and ω_l are the upper and lower limit values of ω, respectively.

To simulate the transient characteristics of ground motions, the envelope function $f(t)$ of intensity is used,

$$f(t) = \begin{cases} t^2/t_1^2 & 0 < t \le t_1 \\ 1 & t_1 < t \le t_2 \\ \exp[-c_d(t - t_2)] & t_2 < t \le T_d \end{cases} \tag{26}$$

where c_d is the attenuation control factor, which ranges between 0.1 and 1.0, and t_1 and t_2 are the first and last moments of the smooth segment, respectively. In this paper, they are set to 2 s and 12 s to ensure that the large acceleration values are within this interval. The duration T_d is set to 20 s. The time-history acceleration series is then obtained by combining $f(t)$ with the stationary Gaussian process $\alpha(t)$ [43],

$$\ddot{x}_g(t) = f(t)\alpha(t) \tag{27}$$

Finally, the target spectrum is used to iteratively adjust C_k to obtain the final earthquake acceleration series,

$$C_{k,i+1} = C_{k,i} \frac{S_\alpha^T(\omega_k)}{S_\alpha^C(\omega_k)},\ i = 0,1,\ldots \tag{28}$$

where $S_a^C(\omega_k)$ is the response spectrum of the generated artificial ground motion.

Based on the preceding process, Fig. 5 shows a group of randomly generated ground motions with peak accelerations of -2.04 m/s^2, -1.50 m/s^2, and 0.95 m/s^2 in the X, Y, and Z directions, respectively. Only this group of ground motions is used in the GSA for the dome because it comprehensively reflects the statistical characteristics of the spectra of natural ground motions.

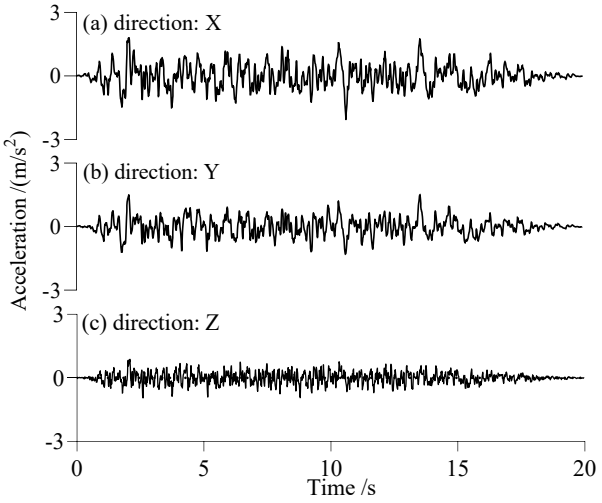

Fig. 5 Reconstructed artificial earthquake ground motions

4.3 Uncertainty quantification for structural performance states

During earthquakes, the members of a lattice dome are subjected to large axial forces and bending moments. The members of the dome are in an elastic state when subjected to minor earthquakes. However,

during major earthquakes, some members may be in an elastoplastic state, while others may be in an elastic state. The proportion r_p of elastoplastic members in the dome is defined to describe the structural performance state,

$$r_p = \frac{N_p}{N_T} \tag{29}$$

where N_p and N_T represent the number of elastoplastic members and total members, respectively. During an earthquake, N_p is determined by the maximum mean strain of the cross-section in the middle of the member exceeding the yielding strain of the steel material. Two elastoplastic states are chosen by adjusting the scale factor of the ground motions. Fig. 6 depicts the quantified distributions of $|D_i|_{max}$ for the three performance states. The mean deformations of the sample domes are 0.0614 m, 0.297 m, and 0.5214 m, respectively. Because the mean deformation of 0.5214 m approaches 1/200 of the span length, which is considered the critical state of collapse in dome structures, the domes in elastoplastic state 2 are on the verge of collapsing. Fig. 7 shows the statistical properties of r_p. It demonstrates that in the defined elastoplastic state 1, some members in almost every dome enter the elastoplastic state, and the mean and standard deviation of r_p are approximately 0.0223 and 0.0155, respectively. For the defined elastoplastic state 2, r_p has a mean value of 0.1022 and a standard deviation of 0.0229. Here, the sample size is set to 4000, which is larger than that in elastoplastic state 1 due to the potentially higher nonlinearities in this state.

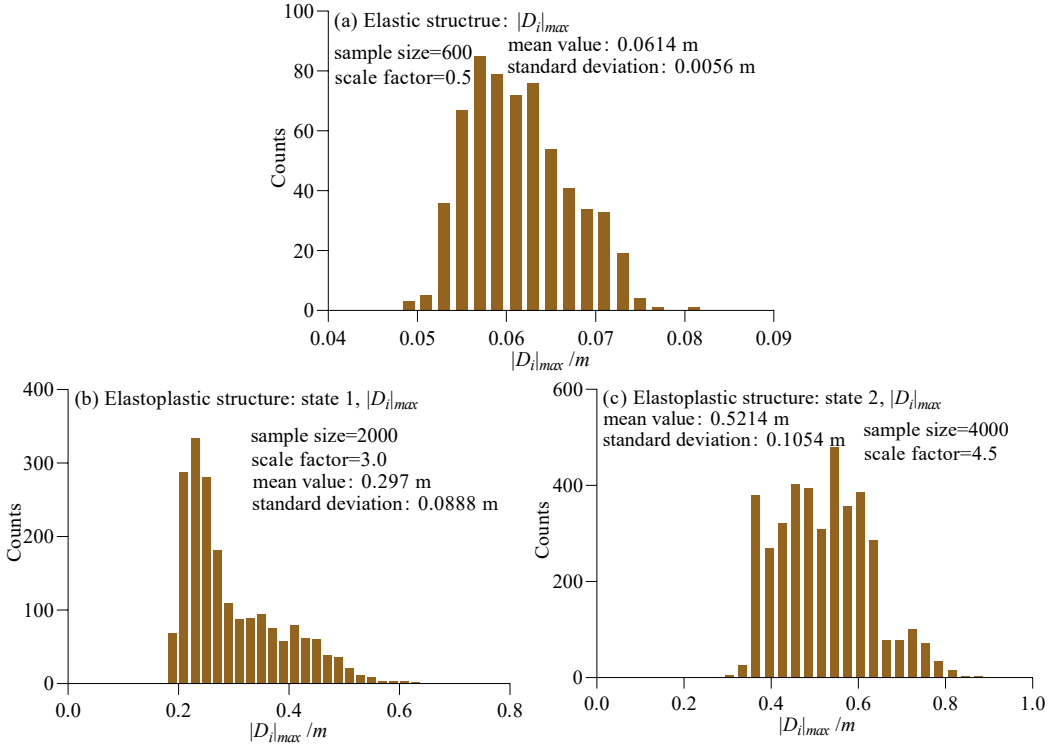

Fig. 6 Three performance states

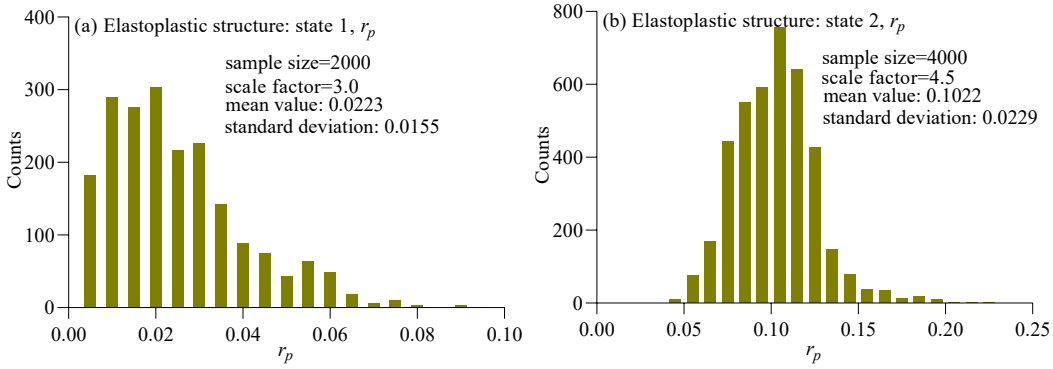

Fig. 7 Two defined elastoplastic states according to r_p

5. Global sensitivity analysis for the dome

5.1 Accuracy of the surrogate model

The accuracy of the surrogate models constructed using the RK method in three states is evaluated, as shown in Figs. 8-10. In the elastic state, the Q^2 values for both the training and test sets are greater than 0.95 using only 600 samples, the *MSE* values of the data are very small, and the regression model is excellent. The predicted values are in good agreement with the observed values according to the test set, because the mean value of error is only 1.26%. As a result, even though geometric nonlinearity exists in the elastic state, a high-accuracy surrogate model can be obtained with small sample size.

For elastoplastic state 1, Q^2 values are greater than 0.9 for both the training and test sets, indicating that the structural nonlinearities reduce the predictability of the dynamic response when compared to the elastic structure. For elastoplastic state 2, Q^2 value on the test set is close to 0.9, and it is extremely difficult to obtain a more accurate surrogate model in this case, which is close to structural collapse with high unpredictability. The mean errors in elastoplastic states 1 and 2 are 5.03% and 5.78%, respectively, which are acceptable in engineering analysis. As previously stated, surrogate models can be used in the structural GSA when the value of Q^2 is greater than 0.8.

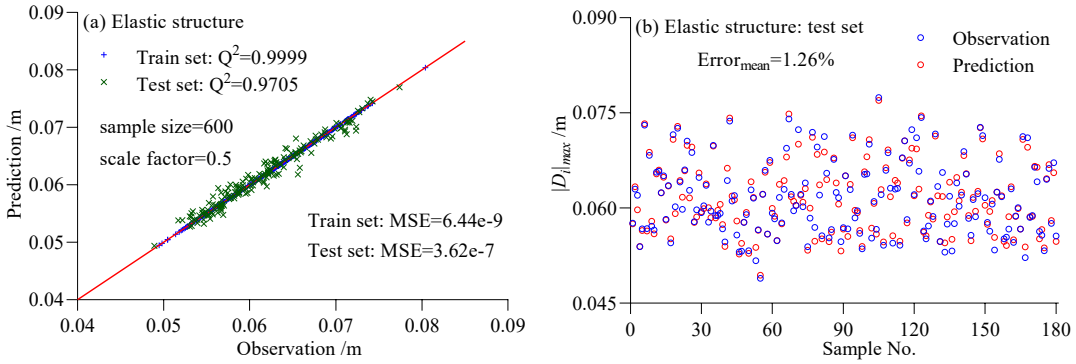

Fig. 8 Assessing the accuracy of the surrogate model for the elastic structure

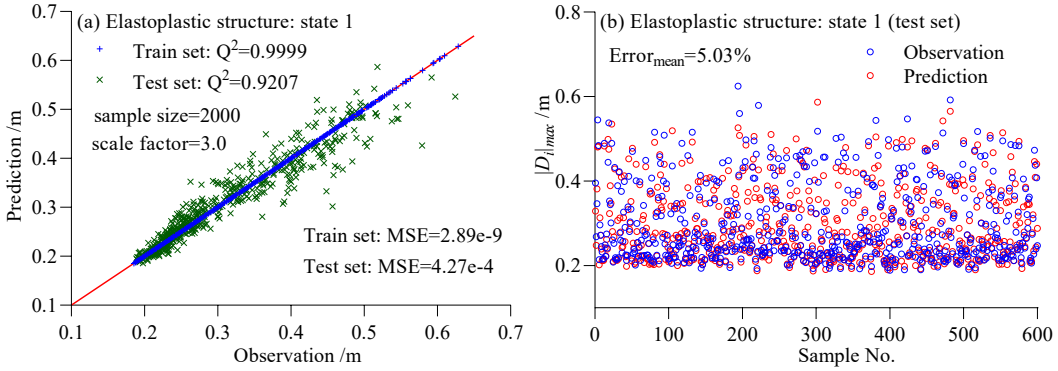

Fig. 9 Assessing the accuracy of the surrogate model for elastoplastic state 1

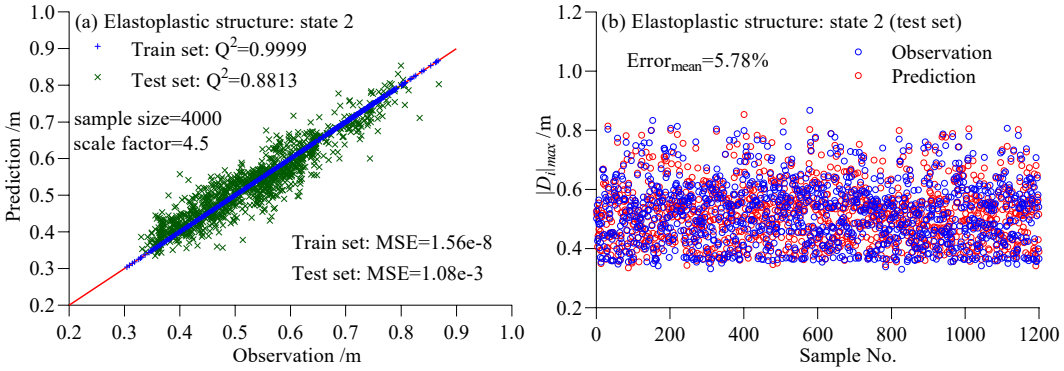

Fig. 10 Assessing the accuracy of the surrogate model for elastoplastic state 2

Using the constructed RK surrogate models and the probabilistic distributions in Table 2, a resampling size of 10000 for the maximum demand are used for each future generation. According to Eqs. (14)-(16), the variance-based sensitivity indices are calculated. In the distribution-based method, the failure samples in generated 50000 samples of the maximum demand are needed to be determined according to Eq. (17). The kernel-smoothed PDFs of the unconditional samples and failure samples are obtained by fitting. The sensitivity index is calculated according to Eq. (18). All results are shown in the following sections.

5.2 Elastic state

The sensitivity index values are estimated using variance- and distribution-based methods with the surrogate model for the elastic state, as shown in Figs. 11 and 12.

•Variance-based sensitivity analysis

Fig. 11(a) shows the estimated values of the first-order and total-order Sobol indices for the single variable using the variance-based method. According to the values, the damping ratio ξ has the greatest effect on the MVD of the structure in this state, followed by the node load N_l, elastic modulus E, and wall-thickness t_w. Because their index values are close to zero, the yield strength f_y and strain-hardening ratio b have almost no effect on the MVD. It should be noticed that the values of the first-order indices of the elastic modulus, wall-thickness of the member, and node load are significantly less than those of the total-order indices, indicating that they interact with other variables.

A single variable may not have a significant effect on the target output of a dome, but in a nonlinear structure, it may have a significant effect through interactions with other variables. The interaction effects between variables are investigated in this paper, as illustrated in Fig. 11(b). The interaction of t_w on N_l has the largest index value S_{ij} in all interactions, followed by the interaction of E on N_l. Other interactions between variables do not affect the MVD due to the small index values.

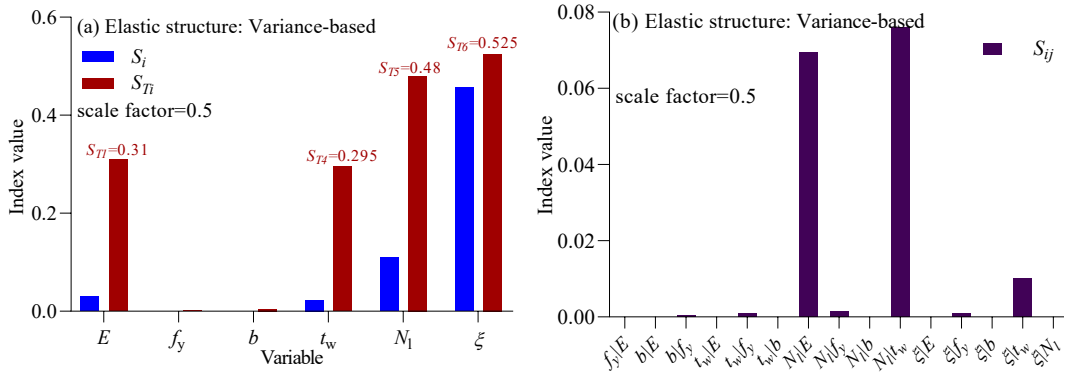

Fig. 11 Variance-based sensitivity analysis of the elastic structure

•Distribution-based sensitivity analysis

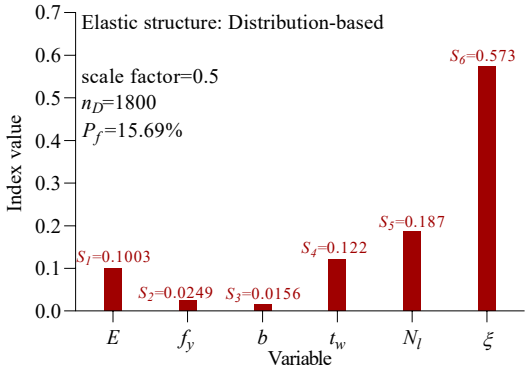

Fig. 12 Distribution-based sensitivity analysis of the elastic structure

The estimated values of indices for the single variables using the distribution-based method are shown in Fig. 12. To determine the failure sample sets of variables, the structural failure should first be defined using Eq. (23). The parameter n_D is set to 1800 in this case, and the failure probability of the structure is approximately 15.69%. According to the index values, the damping ratio ξ has the greatest effect on the failure among all variables for the elastic structure, followed by the node load N_l, wall-thickness t_w, and elastic modulus E. Because their index values are so small, the yield strength f_y and strain-hardening ratio b do not affect structural failure.

5.3 Elastoplastic state

5.3.1 Elastoplastic state 1

•Variance-based sensitivity analysis

Fig. 13 depicts the estimated values of the first-order indices, total-order indices, and interaction effects using the variance-based method. In this state, the damping ratio ξ is still the variable that has the greatest effect on the MVD. The node load N_l, elastic modulus E, and wall-thickness t_w come next. The yield strength f_y and strain-hardening ratio b have the least effects on MVD. According to the values of S_{ij}, the interaction effects of many variables on MVD begin to increase in this state compared to the elastic state. The effects of t_w on N_l and E on N_l remain more dominant than those of other interactions.

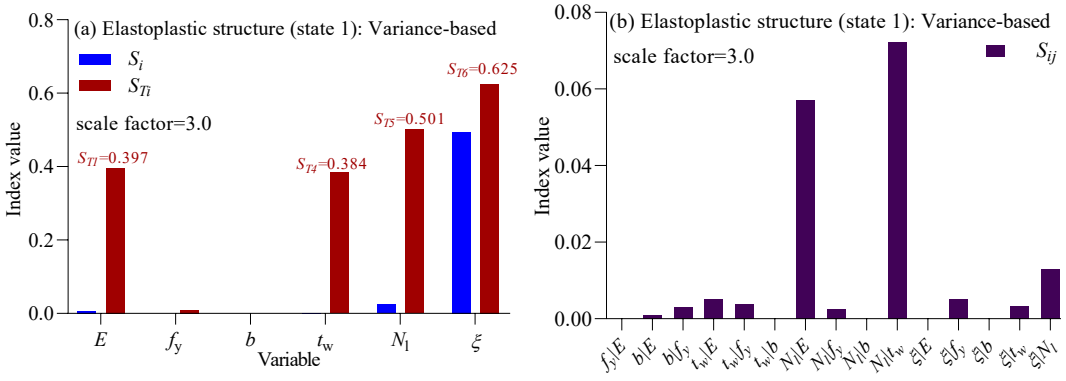

Fig. 13 Variance-based sensitivity analysis for elastoplastic state 1

•Distribution-based sensitivity analysis

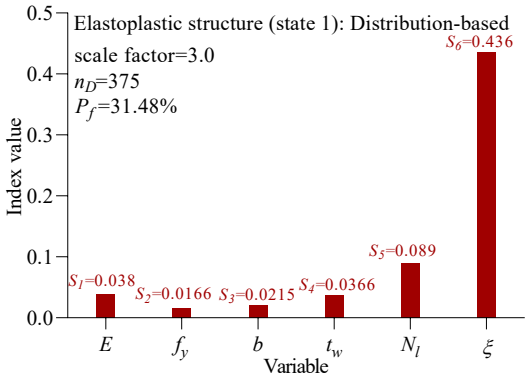

Fig. 14 Distribution-based sensitivity analysis for elastoplastic state 1

The estimated index values using the distribution-based method are shown in Fig. 14, where the constant n_D is set to 375, resulting in a failure probability of 31.48%. The following variables are ranked in order of importance: damping ratio ξ, node load N_l, elastic modulus E, wall-thickness of the member t_w, strain-hardening ratio b, and yield strength f_y. The damping ratio and node load are still two variables with the greatest effect on structural failure, which is consistent with the conclusion obtained through the variance-based method.

5.3.2 Elastoplastic state 2

•Variance-based sensitivity analysis

Fig. 15 shows the estimated index values under elastoplastic state 2 using the variance-based method. According to these values, the effects of the variables on the MVD are completely different from those in the first two structural states. Among all variables, the node load N_l is the most important. It is followed by the wall-thickness t_w, damping ratio ξ, elastic modulus E, yield strength f_y, and strain-hardening ratio b. Despite its low index value, the yield strength f_y has a greater effect on MVD in elastoplastic state 2 than on MVD in elastoplastic state 1. Simultaneously, it is found that the interaction of t_w on N_l are the most significant, indicating that when the dome enters a higher nonlinear state, the effect of this interaction on the MVD should be considered.

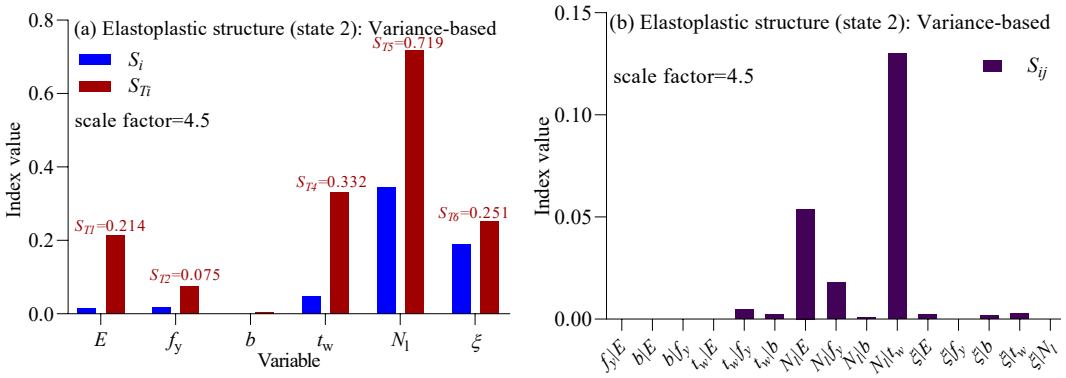

Fig. 15 Variance-based sensitivity analysis for elastoplastic state 2

•Distribution-based sensitivity analysis

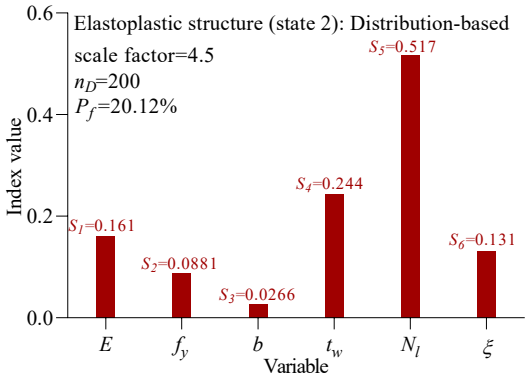

Fig. 16 Distribution-based sensitivity analysis for elastoplastic state 2

Fig. 16 shows the estimated index values using the distribution-based method. The constant n_D is set to 200, resulting in a structural failure probability of 20.12%. The importance ranking of variables is as follows: node load N_l, wall-thickness t_w, elastic modulus E, damping ratio ξ, yield strength f_y, and strain-hardening ratio b, which differs slightly from the importance ranking obtained by the variance-based method. Because of its small value, the effect of the strain-hardening ratio b on structural failure can be ignored.

5.4 Identification of importance and characteristics of variables

The parameter $S_{p,i}$ for the variable $\boldsymbol{x}_i$ is defined to better quantify the effects of each variable on the structural performance in different states,

$$S_{p,i} = S_{Ti}/\sum_{i=1}^{i=n} S_{Ti} \tag{30}$$

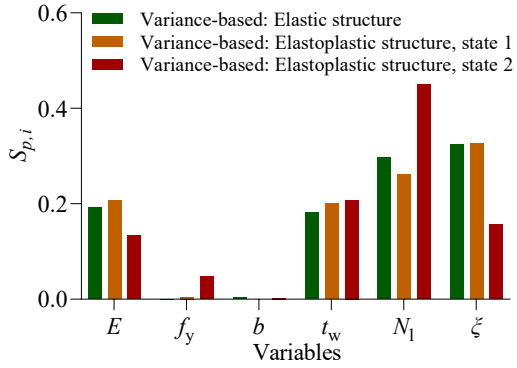

Fig. 17 $S_{p,i}$ of each variable under three states

Based on the previous results, Fig. 17 shows the index $S_{p,i}$ of each variable under three states using the variance-based method. Statistically, the elastic modulus E, wall-thickness t_w, node load N_l, and damping ratio ξ all play important roles in the structural performance for all three states, with the damping ratio ξ and node load N_l dominating in the first two states. The following are the characteristics of the four variables affecting structural performance:

•Elastic modulus E: the importance of this variable in structural performance increases slightly at first, then decreases significantly.

•Wall thickness t_w: the importance of this variable increases slightly as the state transitions from elastic to elastoplastic.

•Node load N_l: it is extremely important in a highly elastoplastic state.

•Damping ratio ξ: the damping ratio plays a critical role in the elastic and slightly elastoplastic states.

5.5 Time-history sensitivity analysis

The sensitivity analysis presented above is based on the MVD ($|D_i|_{max}$) in the structure. However,

there is a maximum vertical deformation at each time t for the i^{th} sample structure, which is denoted as $|d_i|_{max}(t)$, and this physical quantity is time-dependent during an earthquake. The sensitivity of $|d_i|_{max}(t)$ to the variables is discussed in this work. The time-history GSA has not yet been investigated in previous studies.

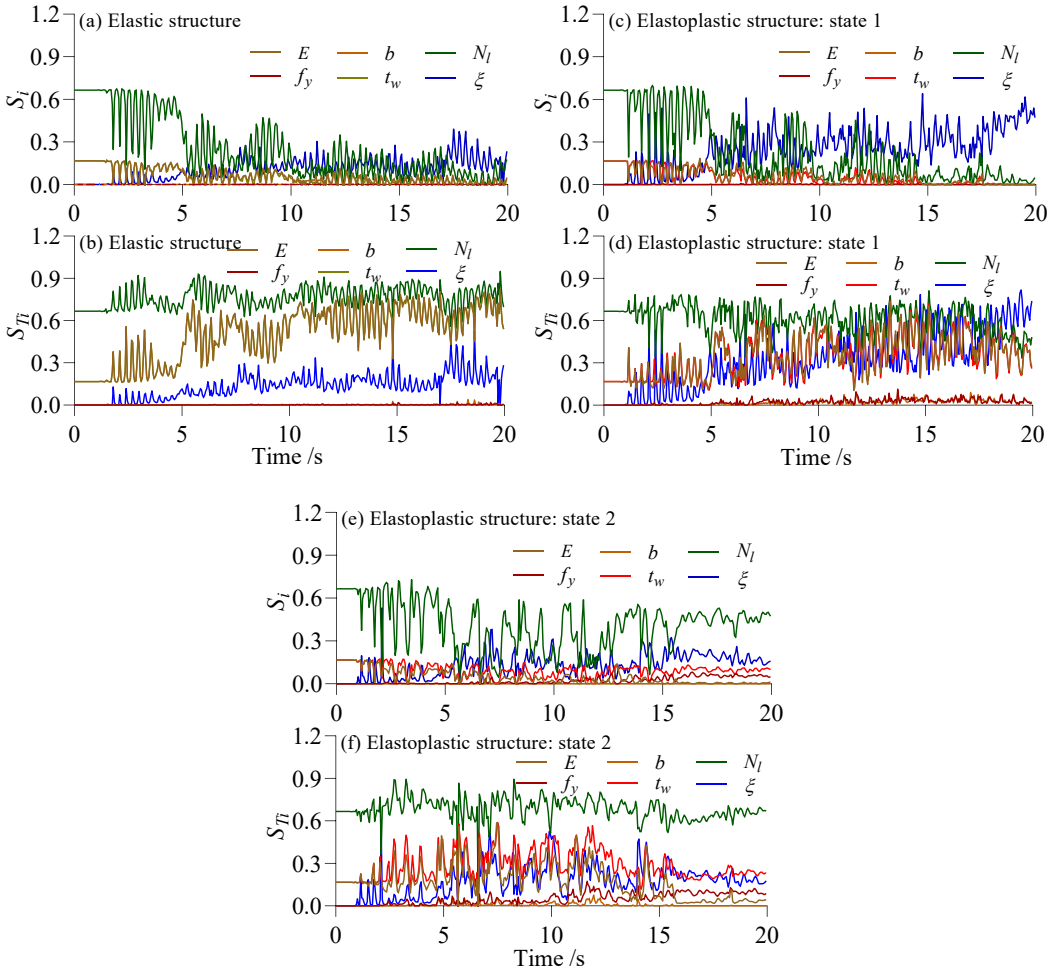

Fig. 18 Time-history sensitivity indices

Fig. 18 shows the estimated values of the time-dependent first-order and total-order indices using the variance-based method. For all sample structures, these values are estimated from $|d_i|_{max}(t)$ at each time t. Because constructing a large number of new surrogate models is a time-consuming task, each estimated index value is output in the intervals of 0.05 s to illustrate the evolution of indices. The total time is 20 s.

Several interesting findings are summarized below:

(1) Because of their large total-order index values, the damping ratio ξ, node load N_l, elastic modulus E, and wall-thickness t_w have noticeable effects on $|d_i|_{max}(t)$ in the first two states, while other variables have little effect. The elastic modulus E and wall-thickness t_w have the nearly identical effect on $|d_i|_{max}(t)$. The values of the first-order indices of the node load N_l, elastic modulus E, and wall-thickness t_w decrease over time, indicating that they interact with other variables.

(2) The index values of the damping ratio ξ increase over time in all three states, especially in elastoplastic state 1, indicating that this variable has a significant effect on $|d_i|_{max}(t)$ in the later stages of the earthquake. This variable has no obvious interaction with other variables in the three

states because the first-order index values are close to the total-order index values. In elastoplastic state 2, the node load N_l has the most important effect on $|d_i|_{max}(t)$. This variable contributes the most to structural deformation.

6. Discussion

6.1 Sensitivity of the surrogate model to sample size

The construction of the surrogate model requires a certain number of samples. A large sample size imposes a significant computational burden, whereas a small sample size cannot fully reflect the relationship between input and output. This paper discusses the effect of sample size on the surrogate model using Q^2 values from the training and test samples, as shown in Fig. 19. To better investigate the sensitivity of the surrogate model to sample size, the scale factor of ground motions is set to 1.0 in this case, and the structure remains elastic.

According to Fig. 19, the Q^2 value increases with sample size, indicating that the surrogate model is sensitive to sample size, particularly in the test set. When the sample size is greater than 400, the surrogate model performs better in terms of generalization. There are currently no effective criteria for determining sample size, which can only be defined by the convergence of statistical quantities. It can be observed that the RK has a good regression ability for the elastic structure when the sample size is larger than 400.

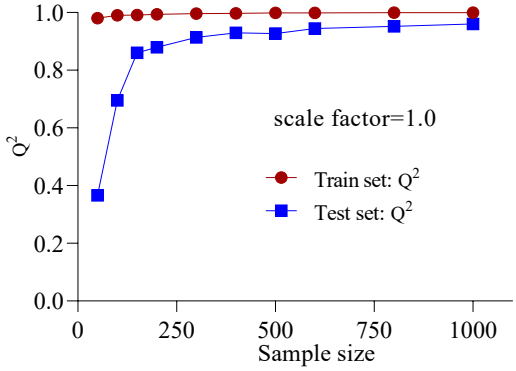

Fig. 19 Sensitivity of the surrogate model to sample size

6.2 A comparison of the accuracy of the surrogate model using different correlation functions

In the RK method, the correlation function influences the accuracy of the surrogate model. Only using the Gaussian correlation function can obtain the surrogate model with the highest accuracy for elastic structures. In this paper, the Gaussian, Matérn 3/2, and Matérn 5/2 functions are compared in surrogate modelling for elastoplastic structures. Fig. 20 shows the Q^2 values and mean errors of two surrogate models on the test sets for elastoplastic state 1. The results show that the Matérn 3/2 correlation function, when compared to the Gaussian correlation function, can improve the surrogate model to some extent, as the Q^2 value increases from 0.9042 to 0.9207, the MSE value decreases from 7.34e-4 to 4.27e-4, and the mean prediction error decreases from 5.57% to 5.03%. However, the Matérn 5/2 correlation function cannot improve the accuracy of the surrogate model.

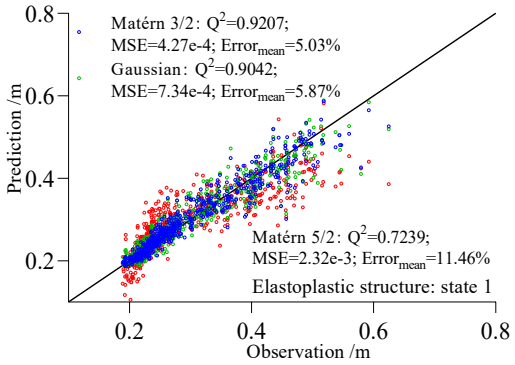

Fig. 20 A comparison between the correlation functions

6.3 Effect of the accuracy of the surrogate model on sensitivity index values

As previously stated, the accuracy of the surrogate model for GSA should be greater than 0.8. The effect of the accuracy of the surrogate model on sensitivity index values is investigated in this paper. Four surrogate models with different accuracy are compared in GSA, and their index values are shown in Fig. 21. The surrogate models with the Q^2 values greater than 0.85 provide nearly identical index values, indicating that these values are stable when the Q^2 values are greater than 0.85. The index values from the surrogate model with the Q^2 value of 0.7110, on the other hand, differ from those of the other three models. It is important to note, however, that the same importance ranking for variables can be obtained using all four models, indicating that the importance ranking of variables is not sensitive to the accuracy of the surrogate model.

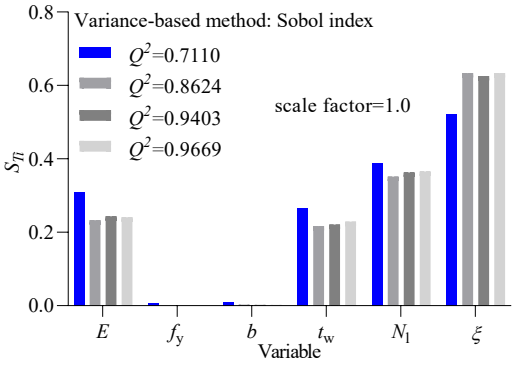

Fig. 21 Effect of the accuracy of the surrogate model on sensitivity index values

6.4 Effect of failure probabilities on distribution-based sensitivity indices

The conditional PDFs of variables must be determined in the distribution-based method based on a failure set. In Eq. (23), the parameter n_D should be assumed in advance. When the probability of structural failure is so low that the kernel smoothing technique cannot accurately fit the conditional PDFs of variables with small samples, the structural GSA may have low accuracy. The effect of failure probability on sensitivity index values is investigated.

Fig. 22 shows the estimated index values of an elastic structure using the distribution-based method for different failure probabilities based on n_D values. Although P_f has no obvious effect on the identification of the importance of variables in the failure probability range of 1.67%-33.22%, it does have a noticeable effect on the estimated index values, which decrease as the failure probability increases. Different failure probabilities result in different target functions (see Eq. (23)), the variables behave differently, and the index values do not remain constant in this case.

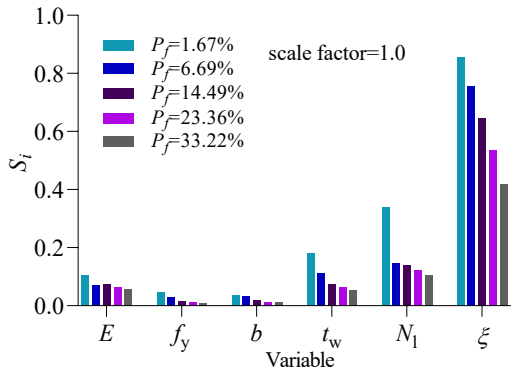

Fig. 22 Effect of the probability of failure on the sensitivity indices

7. Conclusions

The global sensitivity analysis (GSA) plays a critical role in uncertainty quantification of a structure. The conventional finite element method leads to a heavy computational burden in quantifying the effects of sources of uncertainty on structural dynamic performance. In this paper, the regression-Kriging algorithm is used to construct a surrogate model for a large-scale dome structure subjected to earthquake ground motions, thus, the global dynamic behaviours of the nonlinear structure are investigated based on the variance- and distribution-based methods. The results show that the computational efficiency by the proposed method is significantly improved. According to the results, the following conclusions are obtained:

(1) Among the sources of uncertainty related to structures, the damping ratio and roof load are the two most important variables affecting structural performance in both elastic and slightly elastoplastic structures. As the structural plasticity develops, the roof load, rather than damping, plays the most important role. In addition, according to the time-history sensitivity analysis, the index values of the roof load are generally maintained at a high level for three performance states.

(2) The accuracy of the surrogate model is sensitive to the sample size required for the model construction and is affected to some extent by the correlation function used in the RK method. The high-accuracy surrogate model can provide stable sensitivity index values in the variance-based method, whereas the sensitivity index values in the distribution-based method depend on the selection of the failure probability. However, they do not affect the importance ranking of variables.

Acknowledgements

The financial support from the Key Project of the Natural Science Foundation of Tianjin City (Grant No. 19JCZDJC39300) is acknowledged.

References

[1] Zhang HD, Zhu XQ, Yao S. Nonlinear dynamic analysis method for large-scale single-layer lattice domes with uncertain-but-bounded parameters. Engineering Structures, 2020, 203:109780.

[2] Zhang HD, Zhu XQ, Liang X, Guo FY. Stochastic uncertainty quantification of seismic performance of complex large-scale structures using response spectrum method. Engineering Structures, 2021, 235:112096.

[3] Bhattacharyya B. Global sensitivity analysis: A bayesian learning based polynomial chaos approach. Journal of Computational Physics, 2020, 415: 109539.

[4] Wei P, Lu Z, Yuan X. Monte Carlo simulation for moment-independent sensitivity analysis. Reliab. Eng. Syst. Saf., 2013, 110: 60-67.

[5] Gupta HV, Razavi S. Revisiting the basis of sensitivity analysis for dynamical earth system models. Water Resour. Res., 2018, 54: 8692-8717.
[6] Partington D, Knowling MJ, Simmons CT, et al. Worth of hydraulic and water chemistry observation data in terms of the reliability of surface water-groundwater exchange flux predictions under varied flow conditions. Journal of Hydrology, 2020, 590:125441.
[7] Sobol IM, Tarantola S, Gatelli D, Kucherenko SS, Mauntz W. Estimating the approximation error when fixing unessential factors in global sensitivity analysis. Reliab. Eng. Syst. Saf., 2007, 92: 957-960.
[8] Tarantola S, Giglioli N, Jesinghaus J, Saltelli A. Can global sensitivity analysis steer the implementation of models for environmental assessments and decision-making?. Stochastic Environment Research and Risk Assessment, 2002, 16: 63-76.
[9] Razavi S, Jakeman A, et al. The future of sensitivity analysis: An essential discipline for systems modeling and policy support. Environment Modelling and Software, 2021, 137: 104954.
[10] Nariman NA, Hussain, RR, et al. Global sensitivity analysis of certain and uncertain factors for a circular tunnel under seismic action. Frontiers of Structural and Civil Engineering, 2019, 13(6): 1289-1300.
[11] Zoutat M, Elachachi SM, Mekki M, Hamane M. Global sensitivity analysis of soil structure interaction system using N2-SSI method. European Journal of Environmental and Civil Engineering, 2018, 22(2): 192-211.
[12] Menz M, Dubreuil S, et al. Variance based sensitivity analysis for Monte Carlo and importance sampling reliability assessment with gaussian processes. Structural Safety, 2021, 93: 102116.
[13] Zhang KC, Lu ZZ, Wu DQ, Zhang YL. Analytical variance based global sensitivity analysis for models with correlated variables. Applied mathematical modelling, 2017, 45: 748-767. ,
[14] Javidan MM, Kim JK. Variance-based global sensitivity analysis for fuzzy random structural systems. Computer-Aided Civil and Infrastructure Engineering, 2019, 34(7): 602-615.
[15] Arwade SR, Moradi M, Louhghalam A. Variance decomposition and global sensitivity for structural systems. Engineering Structures, 2010, 32(1):1-10.
[16] Boscato G, Russo S, Ceravolo R, Fragonara LZ. Global sensitivity-based model updating for heritage structures. Computer-Aided Civil and Infrastructure Engineering, 2015, 30(8): 620-635.
[17] Zhang XF, Pandey MD. An effective approximation for variance-based global sensitivity analysis. Reliability Engineering & System Safety, 2014, 121: 164-174.
[18] Cucurachi S, Borgonovo E, Heijungs R. A protocol for the global sensitivity analysis of impact assessment models in life cycle assessment. Risk Analysis, 2016, 36(2): 357-377.
[19] Baroni G, Francke T. An effective strategy for combining variance- and distribution-based global sensitivity analysis. Environmental Modelling and Software, 2020, 134: 104851.
[20] Wei PF, Wang YY, Tang CH. Time-variant global reliability sensitivity analysis of structures with both input random variables and stochastic processes. Structural and Multidisciplinary Optimization, 2017, 55(5): 1883-1898.
[21] Ni PH, Xia Y, et al. Using polynomial chaos expansion for uncertainty and sensitivity analysis of bridge structures. Mechanical System and Signal Processing, 2019, 119: 293-311.
[22] Ni PH, Li J, Hao H, Zhou HY. Reliability based design optimization of bridges considering bridge-vehicle interaction by Kriging surrogate model. Engineering Structures, 2021, 246: 112989.
[23] Ni PH, Li J, Hao H, Han Q, Du XL. Probabilistic model updating via variational Bayesian inference and adaptive Gaussian process modeling. Computer Methods in Applied Mechanics and Engineering, 2021, 383: 113915.
[24] Yuan ZX, Liang P, Silva T, et al. Parameter selection for model updating with global sensitivity analysis. Mechanical Systems and Signal Processing, 2019, 115: 483-496.
[25] Wan HP, Ni YQ. An efficient approach for dynamic global sensitivity analysis of stochastic train-track-bridge system. Mechanical Systems and Signal Processing, 2019, 117: 843-861.

[26] Amini A, Abdollahi A, et al. Copula-based reliability and sensitivity analysis of aging dams: Adaptive Kriging and polynomial chaos Kriging methods. Applied Soft Computing, 2021, 109: 107524.
[27] Xian JH, Su C, Spencer BF. Stochastic sensitivity analysis of energy-dissipating structures with nonlinear viscous dampers by efficient equivalent linearization technique based on explicit time-domain method. Probabilistic Engineering Mechanics, 2020, 61: 103080.
[28] Vaezi Vazna R, Zarrin M. Sensitivity analysis of double layer diamatic dome space structure collapse behavior. Engineering Structures, 2020, 212:110511.
[29] Wan HP, Ren WX. Parameter selection in finite-element-model updating by global sensitivity analysis using Gaussian process metamodel. Journal of Structural Engineering, 2015, 141(6): 04014164.
[30] Sun QQ, Dias D. Global sensitivity analysis of probabilistic tunnel seismic deformations using sparse polynomial chaos expansions. Soil Dynamics and Earthquake Engineering, 2021, 141: 106470.
[31] Vu-Bac N, Silani M, Lahmer T, Zhuang X, Rabczuk T. A unified framework for stochastic predictions of mechanical properties of polymeric nanocomposites. Computational Materials Science, 2015, 96: 520-535.
[32] Tuo R, Wang WJ. Kriging prediction with isotropic matérn correlations: Robustness and Experimental Designs. Journal of Machine Learning Research, 2020, 21(1): 7604-7641.
[33] Vu-Bac N, Lahmer T, Zhang Y, Zhuang X, Rabczuk T. Stochastic predictions of interfacial characteristic of polymeric nanocomposites (PNCs). Composites Part B: Engineering, 2014, 59: 80-95.
[34] Liu B, Vu-Bac N, Zhuang X, Rabczuk T. Stochastic multiscale modeling of heat conductivity of Polymeric clay nanocomposites. Mechanics of Materials, 2020, 142: 103280.
[35] Xiao SN, Lu ZZ. Structural reliability sensitivity analysis based on classification of model output. Aerospace Science and Technology, 2017, 71: 52-61.
[36] Fenwick D, Scheidt C, Caers J. Quantifying asymmetric parameter interactions in sensitivity analysis: application to reservoir modeling. Math. Geosci., 2014, 46: 493-511.
[37] Sheather SJ, Jones MC. A reliable data-based bandwidth selection method for kernel density estimation. Journal of the Royal Statistical Society. Series B (Methodological), 1991, 53(3): 683-690.
[38] Marrel A, Iooss B, Laurent B, Roustant O. Calculations of sobol indices for the gaussian process metamodel. Reliability Engineering & System Safety, 2009, 94(3): 742-751.
[39] Sudret B. Global sensitivity analysis using polynomial chaos expansions. Reliability Engineering & System Safety, 2008, 93(7): 964-979.
[40] Liu TT, He Z, Yang Y. Vertical earthquake vulnerability of long-span spherical lattice shells with low rise-span ratios. Engineering Structures, 2020, 207: 110181.
[41] Kaul MK. Stochastic characterization of earthquakes through their response spectrum. Earthquake Engineering & Structural Dynamics, 1978, 6(5): 497-509.
[42] Scanlan R, Sachs K. Earthquake time histories and response spectra. Journal of the Engineering Mechanics Division, 1974, 100(4): 635-655.
[43] Bani-Hani KA, Malkawi AI. A multi-step approach to generate response-spectrum-compatible artificial earthquake accelerograms. Soil Dynamics and Earthquake Engineering, 2017, 97:117-132.